Supplementary Information for manuscript
"Adhesion as a trigger of droplet polarization in flowing emulsions"

Iaroslava Golovkova,[‡] Lorraine Montel,[‡] Franck Pan, Elie Wandersman,
Alexis M. Prevost, Thibault Bertrand, and Lea-Laetitia Pontani[*]

IMAGE ANALYSIS

To identify the droplets on the segmented images and avoid possible artefacts, we only label droplets that have an area larger than 1500 pixels area, a circularity larger than 0.67 and that do not touch the borders of the images. To identify T1 events, we took into account Voronoi cell edges that were not transient and that could thus be detected for at least 4 consecutive frames. A manual inspection of T1 events detected this way shows that only 2% of the detected events are not true T1 events. Of those false T1 events, half of them were caused by segmentation errors, and the other half by exotic 5-cells exchanges of neighbors. When studying droplet deformations, we only consider the droplets whose local packing fraction lies $\Phi_l \in [0.6, 1]$, which allows us to eliminate overlapping or missing droplets resulting from segmentation mistakes. To check the accuracy of the fitted contours, we applied our custom fitting routine to an image of synthetic perfect circles. As shown on Fig. S1 the shape parameter obtained from this model is 1.0009 ± 0.0003, which validates our analysis on real droplets.
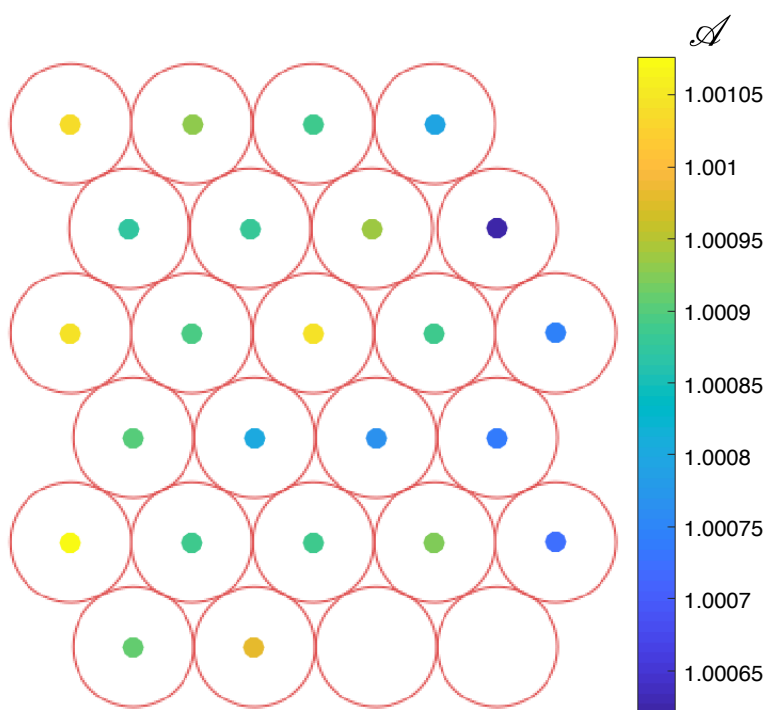

FIG. S1. Synthetic ideal circles and their corresponding calculated shape parameter $\mathcal{A}$, color coded.

TOPOLOGY AND DROPLET REARRANGEMENTS

We define clusters of events, called avalanches, as T1 events neighboring each other within a specified time window $t \pm \Delta t$, where $\Delta t = 0.4$ in adimensional time, which is the time necessary for a droplet to travel 40% of its radius on average. This time window is such that avalanche sizes range from one T1 event to all the droplets contained in the field of view, thus guaranteeing that the rearrangements were not artificially grouped in an excessive time window.

The procedure of distribution of T1 events into separate clusters (i.e. avalanches) is the following. First, for each T1 event, we make the list of all the Voronoi cells that were adjacent to one of the 4 cells of the current T1, at any time point between $t - \Delta t$ and $t + \Delta t$. We then make a list of all the T1 events in which those neighboring cells were involved, within the time window,

and get their cluster identification number (id). If none of the T1 events is already allocated to a cluster id, then a new one is created and given to all the connected T1 events. If all the T1 events have a unique common cluster id, then this id is assigned to the current T1 event. If the T1 events have more than one cluster id, the current T1 event and all connected T1 events are then assigned the smallest of the cluster ids of the list.

DROPLET DEFORMATION

To study the deformation of droplets involved in T1 events, we quantify the difference between the level of droplet deformation $\mathcal{A} = p^2/4\pi a$ before and after a T1 by measuring $\Delta\mathcal{A} = \frac{\mathcal{A}_1^{t^-} + \mathcal{A}_2^{t^-}}{2} - \frac{\mathcal{A}_3^{t^+} + \mathcal{A}_4^{t^+}}{2}$, where $\mathcal{A}_1, \mathcal{A}_2$ are droplets that were in contact before a T1 event, and $\mathcal{A}_3, \mathcal{A}_4$ are droplets that became in contact after the T1 event. t^- and t^+ are the frames just before and after the rearrangement respectively. We find that the distribution of $\Delta\mathcal{A}$ for non-adhesive emulsions is symmetric around a zero value (Fig. S2A), indicating that droplet deformations are identical before and after the rearrangements. In contrast, in the presence of specific adhesion, we observe the increase of higher values of $\Delta\mathcal{A}$ showing that droplets have an excess of deformation prior to a T1 event, which is then released during the exchange of the neighboring droplets (Fig. S2B).
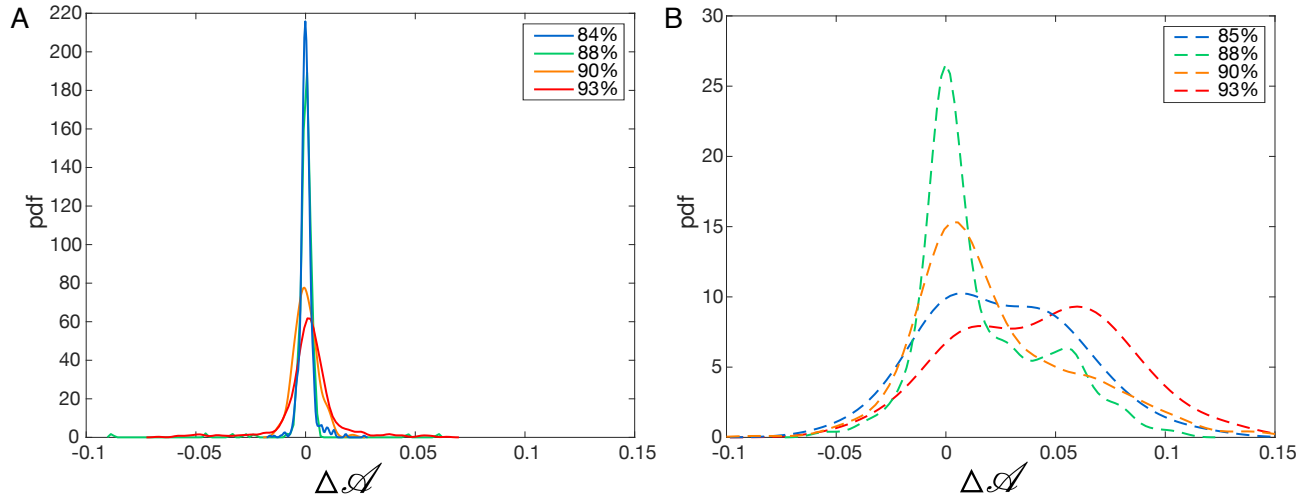

FIG. S2. Probability density function (pdf) of the deformation $\Delta\mathcal{A}$ calculated in the constriction for different packing fractions in the case of (A) non-adhesive and (B) adhesive emulsions. While the distributions for non-adhesive emulsions are symmetrical and centred around zero, the distributions for adhesive emulsions become asymmetrical with a shoulder corresponding to positive values of $\Delta\mathcal{A}$. This shows the accumulation of excessive deformation of adhesive droplets before T1 events, prior to a subsequent relaxation of the deformation after the T1 event.

NUMERICAL SIMULATIONS

Each of the N emulsion droplets is modeled as a deformable polygon with N_v circulo-line edges of width δ. The model relies on the minimization of the following potential energy:

$$U_{DP} = \gamma \sum_{m=1}^{N} \sum_{i=1}^{N_v} l_{m,i} + \frac{k}{2} \sum_{m=1}^{N} (a_m - a_{m0})^2 + U_{int} \tag{1}$$

where $l_{m,i}$ is the length of the circulo-line between vertices i and $i+1$ and a_m is the area of particle m. The first term in U_{DP} is proportional to the perimeter of the droplet with a proportionality constant γ corresponding to a line tension. The second term in this potential energy is a penalization term quadratic in the distance between the area of the droplet and a target area a_{m0}, with a compressibility coefficient k. Finally, U_{int} represents the potential energy of interaction between two droplets, which is composed of the sum of a repulsive term and an attractive term which are given explicitly below (see Fig. S3).

Upon first contact, overlaps between interacting droplets are penalized by introducing a purely repulsive interaction potential
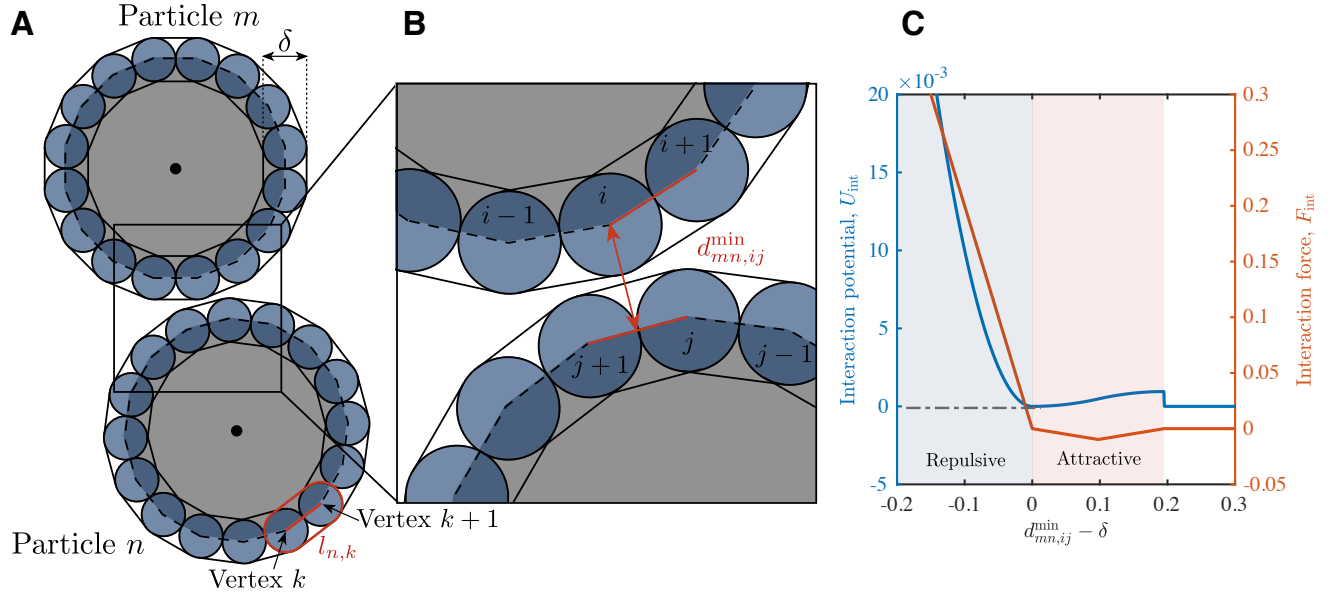
FIG. S3. Schematic of the simulation model — (A) Deformable particles m and n composed of $N_v = 16$ vertices with δ, the length of the circulo-line between vertices k and $k+1$ of particle n is denoted $l_{n,k}$. (B) Close-up on the region of interaction between the two deformable particle, the minimal distance between the circulo-line i on particle m and j on particle n is denoted $d_{mn,ij}^{\min}$. (C) Total interaction potential U_{int} (blue) comprised of a repulsive part U_r and an attractive part U_a which is only applied after particles m and n initiate contact and total interaction force F_{int} (orange). In the limit of non-overlapping particles, the maximum attraction force is small compared to the maximum repulsion force.

U_r between all pairs of circulo-lines. This interaction potential energy reads

$$U_r = \sum_{\substack{m,n=1 \\ m \neq n}}^{N} \sum_{i,j=1}^{N_v} \frac{k_r}{2} \left(\delta - d_{mn,ij}^{\min} \right)^2 \Theta \left(\delta - d_{mn,ij}^{\min} \right), \tag{2}$$

with $d_{mn,ij}^{\min}$ the minimal distance between the circulo-lines i and j respectively on droplet m and n. The Heavyside function $\Theta(x)$ ensures that this potential energy is purely repulsive.

Upon contact, two droplets are also subjected to contact mediated adhesion. For instance, after the initial contact between a vertex of droplet i and a vertex or an edge of droplet j is made, droplets i and j are subject to an attractive force derived from the following potential

$$U_a^{mn,ij} = \begin{cases} k_a h_{mn,ij}^2/2 & \text{if } 0 \leq h_{mn,ij} \leq \delta u \\ -k_a(2\delta u - h_{mn,ij})^2/2 + k_a(\delta u)^2 & \text{if } \delta u \leq h_{mn,ij} \leq 2\delta u \\ 0 & \text{otherwise} \end{cases} \tag{3}$$

where $h_{mn,ij} = d_{mn,ij}^{\min} - \delta$ and u is a parameter controlling the range of the attractive potential. This is then done for all vertices of all pairs of particles in contact. In all our simulations, the range of the attractive potential is kept small with $2\delta u \ll \bar{R}$, where $\bar{R}$ the average radius of a deformable particle. We further ensure that adhesion between vertices is specific, i.e. a given vertex of droplet i can only be subjected to an attraction force from a single vertex or edge from droplet j. Overall, the combined effect of the steric repulsion and the contact-initiated adhesion yields an interaction force which is piecewise linear (see Fig S3).

Note that our model differs from the experimental system in several ways. First, in the experimental setup, adhesion patches are formed progressively, i.e. the adhesion patches are slowly enriched by new biotin-streptavidin-biotin bonds forming at the droplet-droplet contacts, whereas adhesion is instantaneous in the model. In the experiments, this is due to the fact that biotins are free to diffuse at the oil-water interface when they are not part of a biotin-streptavidin-biotin complex. This is the basis of the second difference in between experiments and simulation model: in our toy model, the adhesion forces stem from the vertices, but the position of the vertices determine the shape of the droplet (including its area and perimeter).

Finally, we use in the simulations the same constriction angle as in the experiments. We flow the emulsion through the constriction by subjecting each vertex composing the droplets to a constant force $F_g = 0.002$ in the direction of the channel.
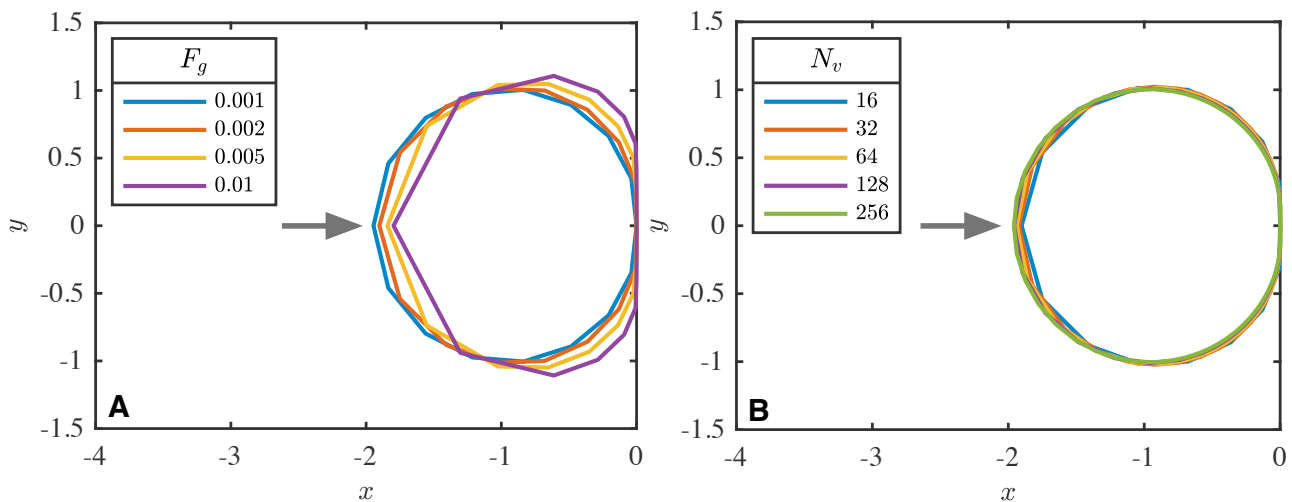
FIG. S4. Deformation of an isolated deformable particle when driven against a flat vertical wall. — (A) A deformable particle with $N_v = 16$ vertices is driven against a vertical wall (in the direction of the grey arrow) with an increasing constant force $F_g = 0.001$ (blue), 0.002 (orange), 0.005 (yellow) and 0.01 (purple). (B) A deformable particle with varying numbers of vertices is driven against a vertical flat wall at constant force $F_g = 0.002$, with $N_v = 16$ (blue), 32 (orange), 64 (yellow), 128 (purple), 256 (green). In all cases, the line tension was $\gamma = 0.1$ and the compressibility $k = 5$ so that our droplets are nearly incompressible and deformations are only accompanied by changes in perimeter.

We illustrate the competition between deformation and the constant driving force F_g by simulating an isolated droplet next to a flat boundary. In Fig. S4, we show the steady-state shapes that our deformable particles adopt for various values of F_g. We use periodic boundary conditions along the axis of the channel, i.e. that droplets exiting the constriction re-enter the channel ahead of the constriction. Provided these forces, we integrate the equations of motion for the vertices in the overdamped limit.

We perform simulations with $N = 128$ deformable particles with $N_v = 16$ vertices per particle and an average radius $\bar{R} = 1$, $\delta = 0.4$ and $u = 0.25$. We vary the line tension $\gamma \in \{0.1, 0.25\}$ and the adhesion strength $k_a \in \{0, 0.01, 0.1\}$ keeping all other parameters fixed for monodisperse emulsions and polydisperse emulsions with 20% polydispersity. We place ourselves in the limit of non-overlapping, nearly incompressible emulsion droplets by using large values for $k_r = 2$ and $k = 5$.

EFFECT OF POLYDISPERSITY ON THE SIZE OF AVALANCHES

In the numerical simulations we examine monodisperse packings and packings with 20% polydispersity, which corresponds to the experimental polydispersity. In each case, we test a range of adhesion strength with $k_a \in \{0, 0.01, 0.1\}$ and a range of deformability by varying the particles line tension $\gamma \in \{0.1, 0.25\}$. We also repeat each simulation five times. We do not observe any significant effect of the adhesion energy on the size of avalanches neither for polydisperse, nor for monodisperse packings, which confirms the results obtained in the experiments. Similarly, deformability does not have any significant effect on the size of avalanches. However, we found that for low-deformability particles ($\gamma = 0.25$), the monodisperse packings exhibit an excess of large avalanches for a given level of adhesion (compare blue, purple and red curves pairwise in Fig. S5).

FLOW VELOCITY

The flow field in the constriction was measured using fluorescent tracer particles of diameter [1-5] μm (GFM, Cospheric, 1.3 g/cm^3, emission wavelength 515 nm). Tracer particles are imaged through fast confocal microscopy (Spinning Disc Xlight V2, Gataca systems) with a 10x objective, and tracked using the FastTrack software [Galois and Candelier, arXiv, 2020]. Their instantaneous velocity was computed as the distance traveled between 2 frames divided by the time between frames. The flow field was then averaged over time to obtain a map of the flow in the constriction which is showed in Fig.S6A. As expected, the flow velocity scales as the inverse of the channel width as shown in Fig.S6B.

- **Supplementary Video 1** : Illustration of avalanche detection in the constriction, for an adhesive emulsion. Each colored disk labels a droplet involved in a T1 event detected in a given time window (8 frames around the T1 event here). Disks of the same color belong to the same avalanche because they are adjacent to one another during the time window.
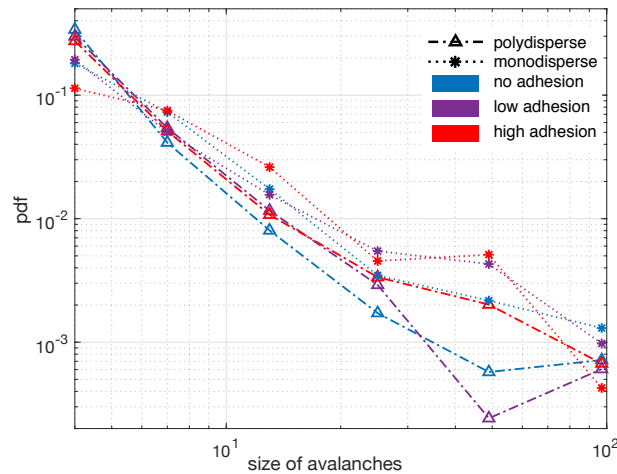
FIG. S5. Probability density function (pdf) of avalanche sizes for simulated packings of polydisperse (dash-dotted lines with triangles) and monodisperse (dotted lines with stars) droplets for three different levels of adhesion. A logarithmic binning as powers of 2 is used. The monodisperse packings exhibit higher avalanche sizes compared to polydisperse packings, for every adhesion level. All conditions are averaged over 5 repeats with the same parameters.
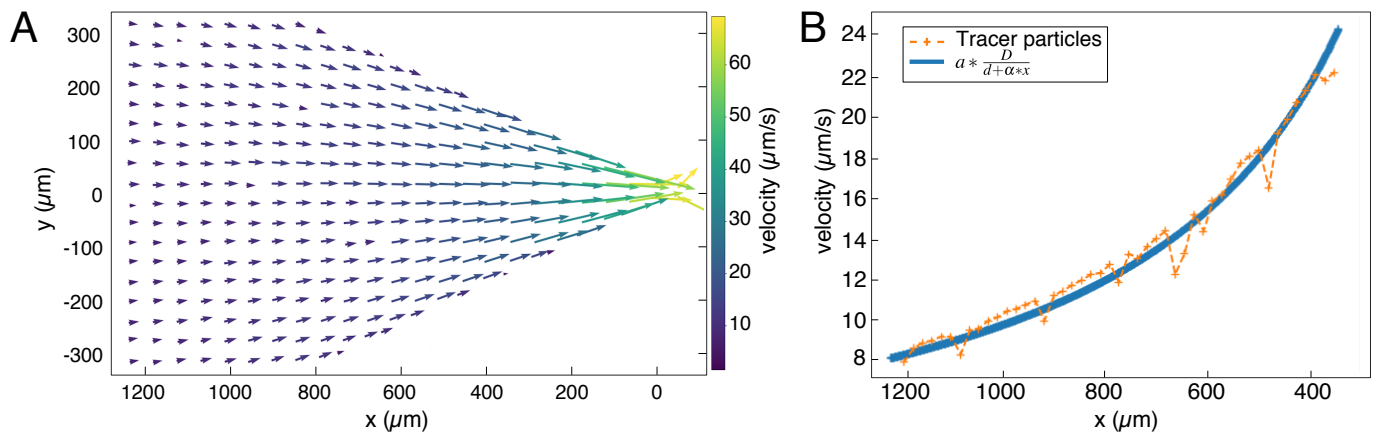

FIG. S6. (A) Flow field in the constriction obtained by tracking tracer particles injected in the channel. (B) Velocity of the tracer particles in the constriction as a function of the distance to the thin channel. The velocity curve is well fitted by an equation taking into account the dimensions of the channel with D=1mm the width of the large channel, d=38 μm the width of the thin one, α= 0.75 degrees the angle of the constriction, and the fitting parameter a = 8.07.

- **Supplementary Video 2** : Movie of adhesive droplets undergoing a T1 event, highlighting the decrease in cell edge length l_e. (Left) confocal imaging of oil droplets labelled with fluorescent streptavidin. (Right) Voronoi tessellation of the droplets. The shrinking cell edge l_e is shown in red.

- **Supplementary Video 3** : Movie of an adhesive emulsion flowed in the constriction and imaged through confocal microscopy.

- **Supplementary Video 4** : Movie of a simulation performed for $\gamma = 0.25$ and $k_a = 0.1$